Predicting Spatial Variability of Sediment Properties From Hydrographic Data for Geoacoustic Inversion

Kerstin Siemes, Mirjam Snellen, Ali R. Amiri-Simkooei, Dick G. Simons, and Jean-Pierre Hermand, *Fellow, IEEE*

***Abstract*—Seafloor classification using acoustic remote sensing techniques is an attractive approach due to its high coverage capabilities and limited costs compared to taking samples of the seafloor. This paper focuses on the characterization of sediments in a coastal environment by combining different hydrographic systems, which are a multibeam echosounder (MBES), a single-beam echosounder (SBES), and seismic systems. The area is located close to the west coast of Italy, southeast of Elba Island, which is known to be composed of very fine-grained material. Both MBES and SBES are, in general, high-frequency systems (>100 kHz), providing bathymetry and backscatter information of the upper part of the sea bottom. MBES systems provide this information with a high resolution, due to the beam opening angle of typically 1°–3°, and high coverage. An SBES provides measurements directly underneath the ship only, but is widespread. For the classification by means of MBES data, we use the Bayesian approach, employing backscatter measurements per beam. For the SBES, echo shape parameters are determined and are combined in a principal component analysis (PCA). Both approaches give results that are in very good agreement with respect to the distribution of different surficial sediment types. Complementary, low-frequency seismic systems (<20 kHz) give insight into the sediment layering. Combining the different acoustic approaches is shown to be an essential ingredient for establishing the environmental picture. This picture is of use for a large range of applications, such as habitat mapping, cable laying, or mine hunting. For the current research, it is aimed to act as a basis for selecting areas for subseafloor sediment classification by geoacoustic inversion techniques. Contrary to the hydrographic systems, geoacoustic inversion techniques provide the actual physical properties, i.e., densities, compression and shear wave speeds, and respective attenuations of the sediment body, and allow sediment characterization over large areas without the need to cover the complete area. A validation is given that the environmental picture, obtained by the hydrographic systems, indeed identifies regions with different acoustic properties.**

***Index Terms*—Environmental characterization, sea bottom sediments, multibeam echosounder (MBES), single-beam echosounder (SBES), seismic profile.**

Manuscript received October 12, 2009; revised June 07, 2010; accepted August 05, 2010. Date of publication November 09, 2010; date of current version November 30, 2010. This work was supported by The Netherlands Organization for Applied Research (TNO) and by the U.S. Office of Naval Research.

Associate Editor: R. Champan.

K. Siemes is with the Acoustic Remote Sensing Group, Faculty of Aerospace Engineering, Delft University of Technology, 2629 HS Delft, The Netherlands and also with the Environmental Hydroacoustics Lab, Université libre de Bruxelles (U.L.B.), 1050 Brussels, Belgium (e-mail: K.Siemes@tudelft.nl).

M. Snellen and D. G. Simons are with the Acoustic Remote Sensing Group, Faculty of Aerospace Engineering, Delft University of Technology, 2629 HS Delft, The Netherlands.

A. R. Amiri-Simkooei is with the Acoustic Remote Sensing Group, Faculty of Aerospace Engineering, Delft University of Technology, 2629 HS Delft, The Netherlands and also with the Department of Surveying Engineering, Faculty of Engineering, The University of Isfahan, 81744 Isfahan, Iran.

J.-P. Hermand is with the Environmental Hydroacoustics Lab, Université libre de Bruxelles (U.L.B.), 1050 Brussels, Belgium.

Digital Object Identifier 10.1109/JOE.2010.2066711

I. Introduction

DETAILED information about the oceanic environment is essential for many applications, such as marine geology, marine biology, and coastal engineering. Also, when evaluating the acoustic propagation characteristics in shallow-water environments, e.g., for sonar performance assessment, the environment needs to be known accurately. This motivates the gathering of information about properties of the water column, the water–sediment interface, and the deeper sediment layers. As a part of an interdisciplinary experimental effort that aims at addressing an integrated concept of Maritime Rapid Environmental Assessment (MREA) [1], this paper focuses on establishing a 3-D picture of the sea bottom sediments. For this purpose measurements with hydrographic systems were employed. These were performed during the MREA/Blue Planet (MREA/BP'07) sea trial, carried out in the Mediterranean Sea, off the Italian west coast and southeast of Elba Island in spring 2007. The combination of the measurements is essential for covering the entire sediment body. The resulting environmental characterization is aimed to serve as a basis for complementary subseafloor sediment characterization techniques, i.e., geoacoustic inversion techniques that also provide the physical properties of the sediment body layers.

The classical technique applied for seafloor material classification is based on taking samples of the sediment. However, these measurements are expensive, time consuming, and provide information at point positions only. Therefore, significant research effort has been dedicated to methods allowing for classification of the sea bottom using acoustic techniques.

A large part of the research on acoustic means for sediment classification has focused on systems that today are widely available, such as multibeam echosounders (MBESs), e.g., [2]–[4]; single-beam echosounders (SBESs), e.g., [5]–[7]; and sidescan sonars (SSSs), e.g., [8]. The advantage of these systems is that they are in use already, and therefore no additional hardware is required. The disadvantage, however, is that these systems typically are mounted on board of a ship, and that sediment information is obtained only for the positions along the ship tracks. In addition, these systems often employ high frequencies in the order of several hundreds of kilohertz, sensing the upper part of the sediment only. Exceptions hold for systems such as the towed ocean bottom instrument (TOBI) [9], operating at a few tens of kilohertz. However, such systems where not available for the current study.

Contrary to these widespread commercially available systems, research has also focused on the use of dedicated systems, such as vertical line arrays spanning a large part of

the water column. Geoacoustic inversion techniques have been developed and have demonstrated to adequately assess the physical properties of the sediments [10]–[15]. Frequencies employed typically lie in the range of several hundreds of hertz, thereby characterizing also the deeper sediment layers. Another advantage of these systems is that the geoacoustic sediment properties, in principle, can be obtained over a large area without the need for a dedicated ship to sail over all parts of interest within the area. However, most of the systems employed in previous research are not suited for application in an operationally relevant context since they are based on relatively complex systems, with e.g., highly instrumented vertical line arrays spanning the entire water column as the receiving system. In the late 1990s, the use of sparse arrays of hydrophones down to a single hydrophone combined with frequency-coherent, model-based matched-filter processing was shown to produce correct geoacoustic parameters [16]. Further experimental work during the MREA/BP'07 experiment demonstrated that geoacoustic inversion results can be operationally obtained using a short array deployed from a small vessel [17] or an underwater robot [18]. For the same purpose, the use of vector sensors is investigated [19].

In this paper, we focus on the use of the commercially available systems for characterizing the seafloor. These are mainly MBES and, for confirmation purposes, SBES systems. To obtain a picture of the entire sediment body, i.e., also of the deeper layer, these high-frequency systems were supplemented by low-frequency seismic measurement systems.

MBES systems have proven to allow for characterization of the seafloor sediments. Many approaches deal with the classification based on MBES backscatter strength data by modeling the backscatter curves along a swath, thereby accounting for scattering at the rough water–sediment interface and volume scattering of the sediment body, e.g., [20] and [21]. When modeling backscatter strengths under different beam angles, the occurrence of nonuniform sediment types within a single swath has to be accounted for. In addition, the MBES needs to be well calibrated, which is not always the case [22]. Therefore, the approach towards sediment classification employing MBES backscatter strength data chosen for this paper employs the backscatter data per beam. It has been developed on the basis of a Bayesian approach as proposed in [23]. To optimize the method for the current application, characterized by water depths ranging from a few meters only to over a hundred meters, modifications to the original method were required.

This paper is organized as follows. Section II gives an overview over the MREA/BP'07 experiment, including information about the survey area, the experimental setup, and the measurement devices employed. Section III deals with the acoustic data (two-way travel time and backscatter strength) obtained by the MBES. Here, backscatter strength data are used for the characterization of the sediments. Then, in Section IV, the echo shape parameters of SBES signals are analyzed by means of a principal component analysis (PCA). In Section V, seismic profiles are presented and analyzed with the aim to obtain a picture of the sediment layering in the entire experimental area. Afterwards, the results from the different measurement devices are compared and interpreted in Section VI. From this comprehensive analysis, regions with comparable acoustic characteristics are detected. In Section VII, the expected acoustic variation among these regions is confirmed for matched-filtered acoustic signals from drifting sparse hydrophone arrays. Finally, the findings are summarized and conclusions are drawn in Section VIII.

II. Description of the Experiment

The MREA/BP'07 sea trial was carried out in the Mediterranean Sea in spring 2007. In the context of the MREA, it aimed at addressing novel concepts of characterizing the underwater environment, thereby investigating means of efficiently obtaining a detailed picture of the underwater environment [17]. For this purpose, a large number of different sensors have been employed. The measured parameters concern both the water column and the sediments. For a detailed description of the experiment, we refer to [1], [24], and [25]. Vessels participating in the MREA/BP'07 experiment were the North Atlantic Treaty Organization (NATO) research vessel (NRV) *Leonardo*, the Italian Ship (ITS) *Galatea* and *Aretusa*, and the His/Her Netherlands Majesty's Ship (HNLMS) *Snellius* of the Royal Netherlands Navy.

The sea trial was located in the BP 3 area southeast of Elba Island and off the coast of Grosseto, Italy, as illustrated in Fig. 1. This region was also a focus of former experiments, such as the Yellow Shark experiments in 1994/1995 [10], [16]. It is part of the shallow continental shelf which links Elba to the Italian peninsula. The shelf was subject to large sediment supplies during the Pleistocene epoch [26]. Today, still large amounts of muddy sediments cover the basement, as documented by core samples, described in the appendix of [16].

In this paper, we focus on those measurements related to the characterization of the sediments, including acoustic measurements and sediment sampling. For an investigation of the water column, we refer to [24] and [25].

An overview of the settings of the acoustic systems is provided in Table I. The measurements considered in this paper were taken in a somewhat smaller region within the BP 3 area, ranging from 10.7° E to 11.0° E and from 42.5° N to 42.8° N, as indicated by the BP 07 rectangle in Fig. 1.

A. MBES and SBES Measurements

Both the SBES and the MBES were mounted on the *HNLMS Snellius* (see Table I). The MBES is a Kongsberg EM3000D dual head, operating at 300 kHz with a selected ping rate of 3–5 Hz. This system has a total opening angle of 130°, within which up to 254 beams are formed. The area surveyed by this MBES is indicated by the dark gray lines in Fig. 1. A similar area is covered by SBES measurements. The SBES system used is a Kongsberg EA600, which delivered data at 200 kHz.

B. Seismic Measurements

Seismic measurements were carried out in the area of the experiment to provide insight into the layering of the bottom. However, due to a tight schedule, the coverage of the MREA/BP'07 area with seismic data is less dense than the coverage with MBES data.

TABLE I
ACOUSTIC DEVICES

Type	Specification	Frequency [kHz]	Beam width [°]	Direction	Ping rate [Hz]
MBES	Kongsberg EM3000D	300 (high)	1.5	normal to grazing	3–5 (max. 40)
SBES	Kongsberg EA600	200 (high)	7.2–15.5	normal	(max. 20)
Seismic	Edgetech X-STAR SB-512i	0.5–12 (low)	16–32	near-normal	(user-selected)
Seismic	Uniboom	0.5–15 (low)	N/A	omnidirectional	1

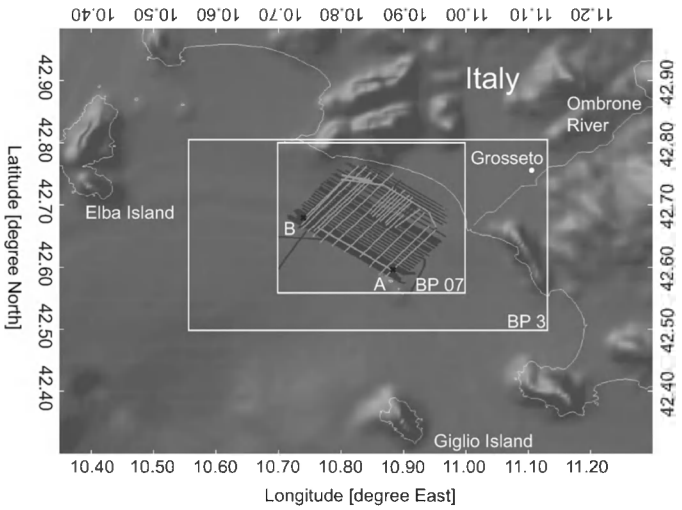

Fig. 1. Overview of the MREA/BP'07 research area. The rectangles mark the BP 3 area and the smaller BP 07 area, respectively. Dark gray lines indicate the tracks of the MBES and the SBES. Light gray lines are the seismic transects of both the X-Star and Uniboom. Background colors indicate the 1 km × 1 km gridded, shaded topography. The topography and coastlines originate from the National Geophysical Data Center [27], [28].

TABLE II
SEDIMENT GRAIN SIZES ACCORDING TO WENTWORTH [29]

M_z [ϕ]	maximum diameter [mm]	sediment
-1–0	2	very coarse sand
0–1	1	coarse sand
1–2	1/2	medium sand
2–3	1/4	fine sand
3–4	1/8	very fine sand
4–8	1/16	silt
8–10	1/256	clay
>10	1/1000	colloid

Two different seismic systems have been worked with (see Table I): the UNIBOOM broadband source (0.5–15 kHz) and the Edgetech X-STAR chirp sub-bottom profiler SB-512i (0.5–12 kHz). The tracks at which seismic profiles are taken with these two systems are shown as light gray lines in Fig. 1. Twelve of these straight lines were sailed with the X-STAR towed behind the *HNLMS Snellius* at a depth of 1.3 m below the sea surface. One of the profiles was taken in the deeper part of the experimental area along the transect AB (which corresponds to the XF transect of the former Yellow Shark experiments [10], [16]). All other X-Star profiles lie perpendicular to this profile, covering both the shallow and deep parts of the MREA/BP'07 area. With the boomer mounted on a catamaran, 16 additional transects were sailed. They again lie perpendicular to the AB transect. However, few transects were also sailed parallel to the coastline in the shallower part of the experimental area.

C. Sediment Samples

Twenty four bottom grab samples have been taken by a Hamon grabber during the experiment. They contain information about the composition of the upper ten centimeters of the seafloor.

A standard criterion to discriminate between different types of sediments is their grain size. Grain size is either given in millimeter or ϕ units, which are related according to

$$d = -\log_2 D. \tag{1}$$

Here, D denotes the grain diameter in millimeters and d is the corresponding value in ϕ units. For the description of the different grain sizes, we follow the nomenclature of Wentworth [29], as given in Table II.

For each grab sample, the mean grain size M_z in ϕ units is calculated, according to [30], as the average over the three grain sizes d_{16}, d_{50}, and d_{84}, at which 16%, 50%, and 84% of the grains are smaller, respectively

$$M_z = \frac{d_{16} + d_{50} + d_{84}}{3}. \tag{2}$$

The sediment distribution obtained from the grab samples is given in Fig. 2. It mainly agrees with historic cores taken in this area, as described in the appendix of [16]. The grab samples indicate very fine sediments with mean grain sizes of $M_z = 7\phi$ to $M_z = 11\phi$, which equal a grain diameter of 0.008 mm and less. The finest sediments with $M_z = 11\phi$ occur in the deepest parts of the MREA/BP'07 area, while the somewhat coarser sediments with $M_z = 7\phi$ settle close to the coast. The mean grain sizes are depicted in Fig. 2 as the diameter of the symbols. Also, the percentages of the sand, silt, clay, and colloid contribution of the upper sediment layer, calculated from all particles within a sediment sample, are shown. From these, it can be concluded that the contribution of the finer sediment slightly increases from the shallow to the deeper part.

III. MBES ANALYSIS—METHODS AND RESULTS

MBESs send out pulsed acoustic signals and measure both the (two-way) travel time and the strength of the scattered received signal for a large number of beams. Bathymetry is obtained from the (two-way) travel time as measured from the MBES per beam. The backscatter strength strongly depends on properties of the sediments such as surface roughness, density, sound speed, and volume inhomogeneties. Therefore, it can be

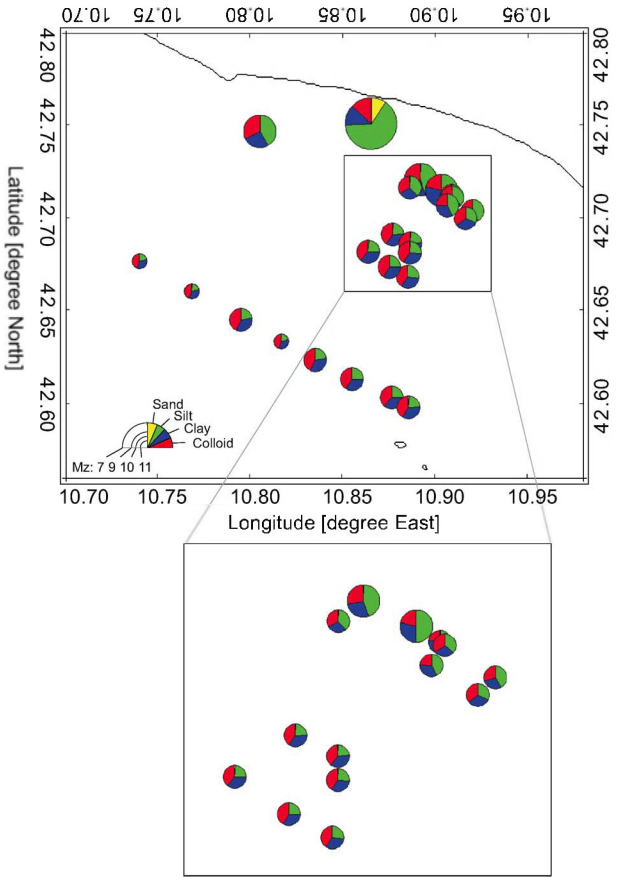

Fig. 2. Sediment distribution in the MREA/BP'07 experimental area obtained from the analysis of grab samples taken during the experiment. This figure presents two parameters that describe the sediment type. One is the composition (sand, silt, clay, and colloid) of the sediment samples, given as pie charts, thereby accounting for all particles within a sample. The other is the mean grain size M_z of the sediment, calculated according to (2) and rounded to integer values. M_z is indicated by the diameter of the symbols, which is reciprocally proportional to its value.

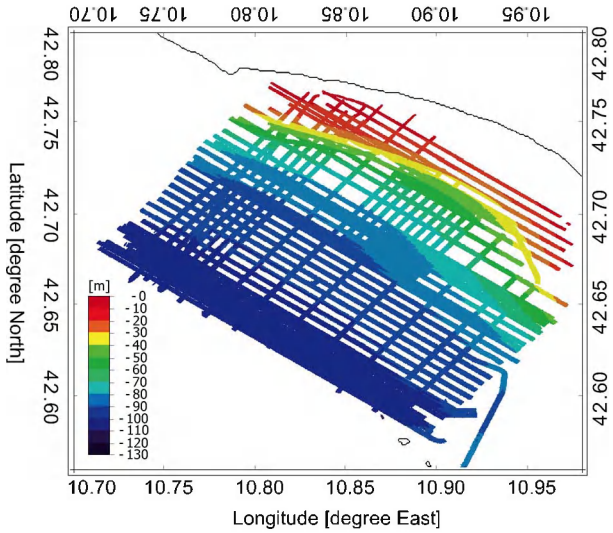

Fig. 3. Bathymetry in the MREA/BP'07 experimental area obtained from MBES (two-way) travel time measurements (fully corrected for ship attitude and water-column properties).

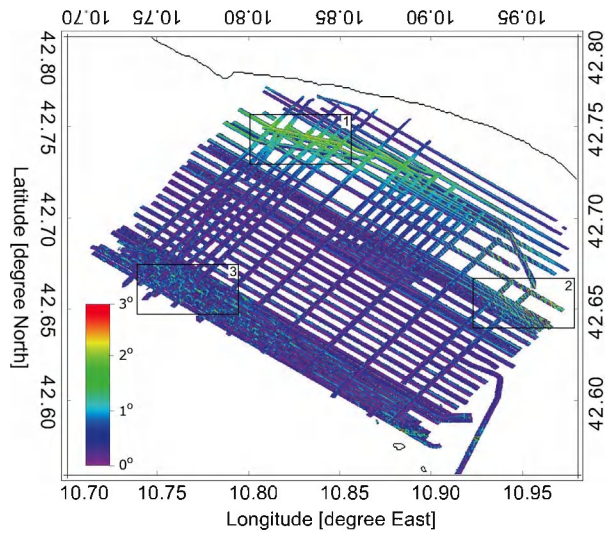

Fig. 4. Slope in the MREA/BP'07 experimental area: 1) continuously increased slope; 2) regular structure; 3) irregular structure.

employed for sediment characterization. Due to the high frequency used (300 kHz), the absorption length amounts to half a meter at maximum even for the prevailing fine-grained sediments (7–11 ϕ). Therefore, the MBES data are not influenced by properties of the sediment body (deeper than 25 cm), such as sediment layering.

A. *Bathymetry*

Depth values cover the wide range of a few meters to approximately 130 m, as can be seen in bathymetry map (Fig. 3). Starting at approximately 10 m in the shallow coastal area in the north, depth increases with the distance to the coast and shows isobaths that tend to follow the coastline. At 15-km distance to the coast, the deepest part of the MBES survey is reached.

Generally, the change in depth per unit of distance is small, except for a small region near the coast (between 20- and 40-m depth). This is shown in Fig. 4, presenting the slopes as a function of position. In general, slope values of the MREA/BP'07 experimental area lie below 1°. At some locations, such as the above mentioned regions, they are slightly increased, but do not exceed 3°. Contrary to the bathymetric map, the map of slope values shows more texture. Three distinct regions can be discerned. The first one is the region of transition from the shallow to deeper parts in the north, which shows slightly higher slope values. A second region in which high values for the slopes are present lies close to the Ombrone estuary in the east, at water depths less than 70 m. Here, the slope values indicate the presence of a regular structure, which is orientated parallel to the isobaths. In the third region, an irregular, inhomogeneous structure can be found in the deep, western part of the research area, which features the softest sediments of the experimental area (see Section II-C).

B. *Mapping the Acoustic Classes*

For characterizing the seafloor sediments, we use the backscatter strengths derived from the intensity of the backscattered acoustic signal. The approach selected for the current research utilizes the averaged backscatter strengths per beam.

An advantage of this approach is its insensitivity to variations of seafloor type along the swath. In addition, imperfect calibration of the MBES system does not hamper the classification. The approach is presented in [23]. For the current research, it is extended. In [23], classification results, based on the MBES backscatter strengths, were presented when only a single beam was employed for the classification. Due to the relatively large distances between the tracks covered by the MBES for the data considered here, the method was modified such that a large number of beams were accounted for in the classification, thereby exploiting the high coverage capacity of the MBES. In addition, the MREA/BP'07 area exhibited large variations in depths. This resulted in more variations (over the area) in statistical properties of the averaged beam backscatter strengths. To properly account for these variations, a further extension was required as described in the following.

1) Classification Method: The present geoacoustic classification method is based on the Bayesian approach as applied in [23]. It assumes that the filtered backscatter value BS_θ, as provided by the MBES system at beam angle θ, is the average of N_θ backscatter strength values $\mathrm{BS}_{\theta,n}$ obtained from $n = 1, \ldots, N_\theta$ scatter pixels within the beam footprint at θ

$$\mathrm{BS}_\theta = \frac{1}{N_\theta} \sum_{n=1}^{N_\theta} \mathrm{BS}_{\theta,n}. \tag{3}$$

Theoretically, the available number of scatter pixels can be determined from the beam geometry (Fig. 5) as the fraction of the size of the beam footprint dA and the size of a scatter pixel da

$$\begin{aligned} N_\theta &= \frac{dA}{da} \\ &= \frac{H\theta_T}{\cos^2(\theta)} \times \frac{2\sin(\theta)}{c\tau} \end{aligned} \tag{4}$$

which varies with the water depth H, the beam angle θ, and the beam opening angle θ_T, which also depends on θ. The variables c and τ denote the water-column sound speed and the pulse length, respectively. While (4) is valid for beams away from nadir, $N_{\theta=0} = 1$ holds at nadir.

If the number of scatter pixels for averaging per beam footprint is large enough, the central limit theorem holds, resulting in BS_θ being normally distributed. When a single seafloor type is present, this allows one to fit a single Gaussian probability density function (pdf) to the histogram of observed backscatter strength at that angle. If more than one (namely m) seafloor type is present, the backscatter histogram can be modeled by a sum of m scaled Gaussians

$$\begin{aligned} f(\mathrm{BS}_\theta|x) &= \sum_{k=1}^{m} f(\mathrm{BS}_\theta|x_k) \\ &= \sum_{k=1}^{m} c_k \exp\left(-\frac{(\mathrm{BS}_\theta - \mu_k)^2}{2\sigma_k^2}\right) \end{aligned} \tag{5}$$

as depicted in Fig. 6. Here, for each Gaussian pdf, $f(\mathrm{BS}_\theta|x_k), x_k = [c_k, \mu_k, \sigma_k]^T$ holds, with c_k the scaling factor, μ_k the mean, and σ_k the standard deviation of the kth pdf. The unknown parameter vector $x = [x_1, x_2, \ldots, x_m]^T$ can

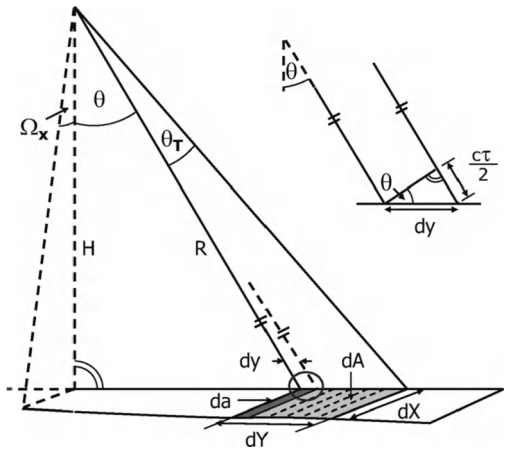

Fig. 5. Schematic of the beam- and signal footprint of an MBES as obtained by the receiver array. The beam footprint $dA = dX \times dY$ and the footprint of scatter pixel $da = dX \times dy$ are indicated in lighter and darker gray, respectively. They depend on the beam angle θ, the beam opening angle in across-track direction θ_T (related to θ), the beam opening angle in along-track direction Ω_X, and depth H (or alternatively range R). The upper right plot zooms into a single scatter pixel. Here, c is the water-column sound speed and τ is the pulse duration.

be estimated using the least squares technique. The nonlinear least squares, subject to bounds on variables [31], is used to obtain the μ_ks and σ_ks, and the nonnegative least squares method [32] is used to obtain the contributions of the individual pdfs by constraining the coefficients c_ks to be positive. For further explanation of the method and the steps involved, we refer to [23].

This approach is well suited for regions with a uniform and moderate depth. However, the assumption of a normal distribution for the averaged backscatter strength does not hold, if the number of scatter pixels is small. Especially in very shallow water and at low beam angles θ, beam footprints contain too few scatter pixels. Therefore, a modification is applied to the above described classification method which involves an averaging over both beams and pings, to create regions with comparable large numbers of independent scatter pixels. The averaging over beams involves a number of $b = b(\theta)$ beams, which again depends on the beam angle. Close to nadir, a small number of scatter pixels per beam footprint demands averaging over a large number of beams. At the outer beams, where beam footprints are large, b has to be chosen smaller. This ensures a comparable number of scatter pixels both at low and high incident angles.

In [33], this approach has been applied to MBES data taken in a very shallow (<5 m) river environment. It was demonstrated that averaging indeed restored Gaussianity of the beam backscatter values.

For a given depth H, (4) gives a rough estimation for the number of beams used in the averaging as

$$b = \frac{\cos^2\theta}{\sin\theta}. \tag{6}$$

Taking the b beams into account, they span an angular range of θ_{tol} as shown in Fig. 7. More precisely, one has to include all beam angles around the central beam angle θ as: $\theta - \theta_{\mathrm{tol}}/2 \leq \theta \leq \theta + \theta_{\mathrm{tol}}/2$. The values of these angular ranges θ_{tol} are determined from (6) and used as tolerances. Typical values used

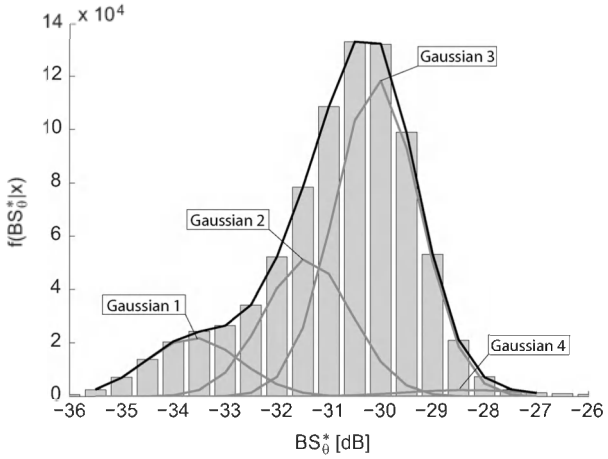

Fig. 6. Fitting four Gaussians (gray curves) to the histogram of all backscatter strengths at 46° beam angle. The black curve gives the sum of the four Gaussians.

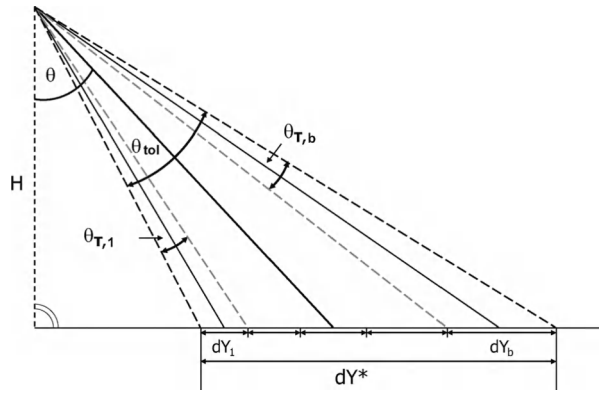

Fig. 7. Angle of tolerance θ_{tol}. Within this angle all scatter pixels from all beams $\theta_{T,1}, \ldots, \theta_{T,b}$ are taken into account for averaging. Here, $dY_k, k = 1, \ldots, b$ denote the across-track size of the b footprints, respectively, and dY^* is the across-track size of the footprint dedicated to θ_{tol}.

TABLE III
PARTITION OF BEAM ANGLES AND RELATED TOLERANCE ANGLE (θ_{tol}) FOR AVERAGING OVER BEAMS

angular range [°]	θ_{tol} [°]
$\theta \geq 38$	2.5
$38 > \theta > 24$	4.4
$24 \geq \theta \geq 20$	6.4

in this contribution are listed in Table III. Based on the fact that the number of scatter pixels at angles smaller than 20° is too small to result in reasonable tolerance angles, these angles are not considered for classification.

After having decreased the angular dependence, we expect that the number of scatter pixels per beam footprint still varies with depth. Therefore, an averaging over $p = p(H)$ pings is proposed in the next step as discussed in [34]. The number of pings involved in this averaging process depends on the water depth H and is determined empirically by comparison of number of scatter pixels at different water depths. The values used in this contribution are presented in Table IV.

TABLE IV
PARTITION OF DEPTH VALUES AND RELATED NUMBER OF PINGS FOR AVERAGING (p)

depth range [m]	p [-]
<10	12
10-15	8
15-20	6
20-25	4
25-35	3
35-80	2
>80	1

Averaging over b beams and p pings results in the following backscatter strength values:

$$\text{BS}^*_\theta = \frac{1}{p}\frac{1}{b}\sum_{l=1}^{p}\sum_{\theta\in\theta_{\text{tol}}} \text{BS}_{\theta,l}. \tag{7}$$

The averaged backscatter strengths BS^*_θ are now assumed to have a normal distribution, since large numbers of scatter pixels contribute to BS^*_θ. They are employed for classification, using the Bayesian approach for single beams, with beam angles in the range of $\theta_1, \ldots, \theta_r$.

From the classification at low grazing angles (i.e., large beam angles, being reference angles $\theta_1 = 46°, \theta_2 = 44°$, and $\theta_3 = 42°$), the number of classes m is determined, since a better discriminating performance is expected at these angles. In principle, we expect the backscatter values measured at other angle ranges to correspond to the same number of classes. Therefore, we assume m to be constant for the considered range of beam angles: $\theta_1, \ldots, \theta_r$.

Additionally, the three initial classifications provide us with the μ_ks, σ_ks, and c_ks for the three reference angles. The mean values (over all reference angles) of the Gaussian pdf parameters can then be obtained: $\bar{\mu}_k, \bar{\sigma}_k$, and $\bar{c}_k (k = 1, \ldots, m)$, as shown in Fig. 8(a).

For application of the classification method to an arbitrary angle under study (θ), we use the fixed number of classes that has been obtained from the classification at the reference angles. First, the entire histogram of the averaged backscatter strengths BS^*_θ of the angle under study is shifted such that the mean of BS^*_θ becomes identical to the mean of the averaged backscatter strengths at reference angles (θ_1, θ_2, and θ_3). As an initial guess for the mean values of the Gaussian pdfs, we use $\bar{\mu}_k (k = 1, \ldots, m)$ of the reference angles. Then, more restricted bounds on the mean parameters are used in the least squares process, e.g., $\mu^l_k = \bar{\mu}_k - 0.5$ dB for the lower bound and $\mu^u_k = \bar{\mu}_k + 0.5$ dB for the upper bound. Results for beam angles of 40° and 38° are depicted in Fig. 8(b).

2) Classification Results: The application of the Bayesian approach to the MBES data results in four classes for the considered angular range of $\theta_1 = 46°$ to $\theta_r = 26°$ beam angle. Larger beam angles could not be accounted for, since for these angles the backscatter signals were too weak to be detected in the deeper parts of the experimental area. Also, beams near normal incidence are not considered for classification, since they contain too few scatter pixels to assume normally distributed backscatter strength.

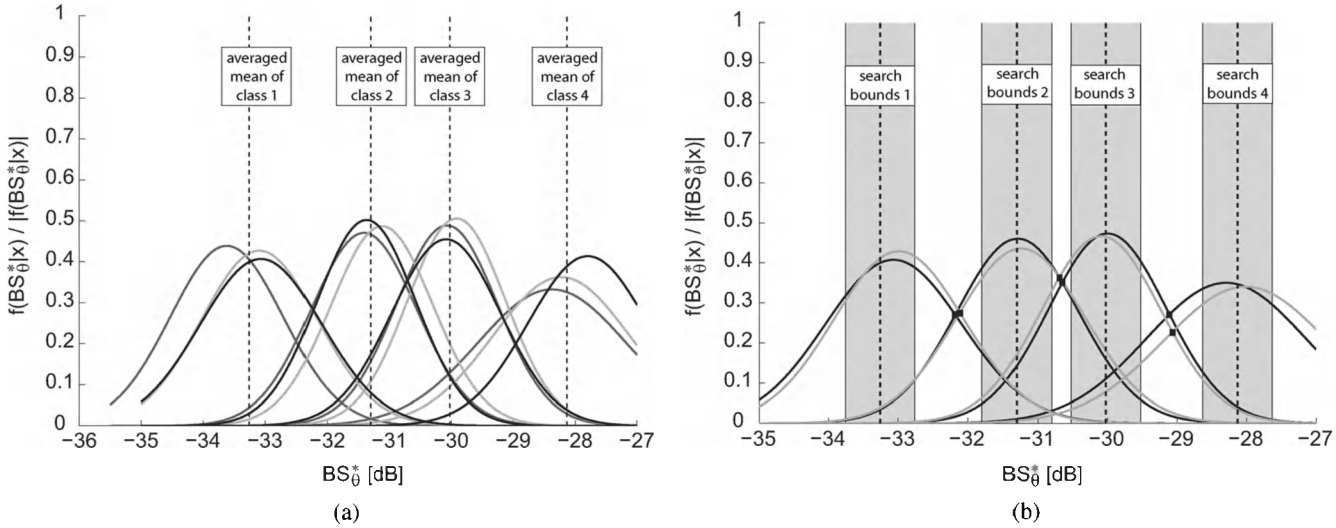

Fig. 8. Normalized Gaussians (a) at the reference angles and (b) at arbitrary angles. In (a), reference angles are chosen as 46° (light gray), 44° (black), and 42° (medium gray). Per angle, the four Gaussians are plotted as estimated by the Bayesian approach for single beam angles. For each class, the average of the Gaussian means is indicated by a vertical dashed line. According to the reference angles, a shift in backscatter strength is applied for all beam angles. Then, the Gaussian mean values at an arbitrary angle are restricted to a boundary of ±0.5 dB around the averaged means obtained at the reference angles. These boundaries are shown in (b) as gray rectangles. Here, classification has been applied to shifted backscatter strength at beam angles of 40° and 38°, indicated by the black and gray curves, respectively. Class boundaries are given by the intersection points (black squares) of the normalized Gaussians.

Fig. 9 presents the results. We can identify clearly separable areas, each belonging to a single class. The highest backscatter strengths are found in the shallowest part, close to the Italian coast. Lowest backscatter strengths occur in the area with water depths of approximately 40–60 m. Then, with increasing depth, also backscatter strength increases again. However, a somewhat asymmetric distribution between the northern and southern parts can be observed at comparable depth. In several areas, a coexistence of two classes can be observed. Some of these areas coincide with areas identified by particular slope patterns. For example, this holds for the region close to the Ombrone estuary in the eastern part, where a regular structure is found in both the slope map (Fig. 4) and the map of backscatter strength classes (Fig. 9). Also for the irregular structure in the deeper southwestern part, the influence of a second backscatter strength class is revealed to some degree, by showing an additional increase in backscatter strength at the outer beam angles at several locations. Since this behavior is not clearly visible in the other areas, it is hypothesized that the backscatter behavior can be related to geomorphologic features, already visible in the slope map. Additionally, small-scale structures can be recognized in the center of the MREA/BP'07 area, which could not be resolved in the slope map.

IV. SBES Analysis

The objective of this section is to investigate the echo shape parameters of the SBES signals, as reflected at the seafloor and received by the transducer, to discriminate between different sediment types [35].

The SBES system transmits an acoustic pulse towards the sea bottom and determines the water depth from the (two-way) travel time of the signal. Several features of the received signal, such as total energy, time spread, and skewness, contain information on the sea bottom composition. These features are conceptually similar to the first, second, and third statistical moments. Such features can potentially be used for seafloor classification [35].

Although the three features (energy, time spread, and skewness) are intrinsically different in nature, they are statistically correlated. The PCA is adopted according to [36] to reduce the dimensionality of the extracted features while retaining most of the variation of the features. The PCA transforms a number of different but possibly correlated variables via linear combination into a smaller number of uncorrelated variables, called principal components. The first principal components account for as much of the variability in the data as possible. They are then fed to a cluster analysis based on the well-known K-means clustering algorithm [37].

For this analysis, SBES data obtained at a frequency of 200 kHz are chosen, which is comparable to the frequency of 300 kHz of the MBES system. The sample rate of the SBES amounts to about 15 kHz, sufficient for accurately estimating the echo shape parameters. The intensities of the received signals have been corrected for spherical spreading and footprint effects. Another depth-dependent correction scales the echoes in time in relation to a given reference depth. This correction compresses signals that are obtained at a depth greater than the reference depth and elongates signals from a depth smaller than the reference depth.

The three signal features have been extracted from the recorded signals. Then, the features have been normalized such that each echo feature has a zero mean and unit variance. For each extracted feature, the noise level has been reduced by averaging over 40 consecutive pings. All three resulting parameters show correlations, as displayed in Table V. Especially, the energy and time spread are highly correlated.

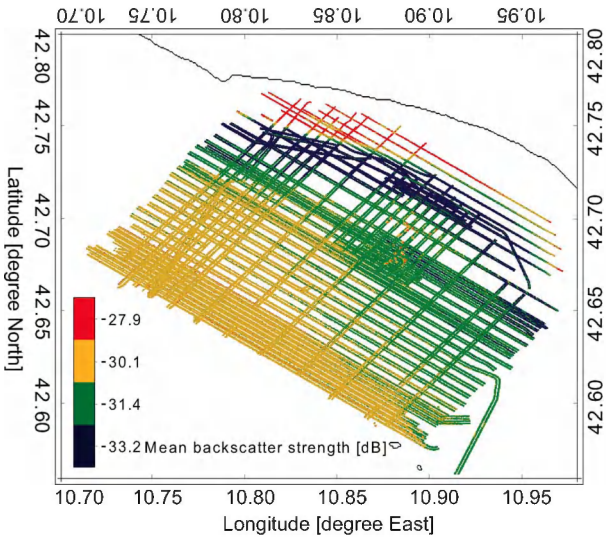

Fig. 9. Map of the four MBES backscatter strength classes derived.

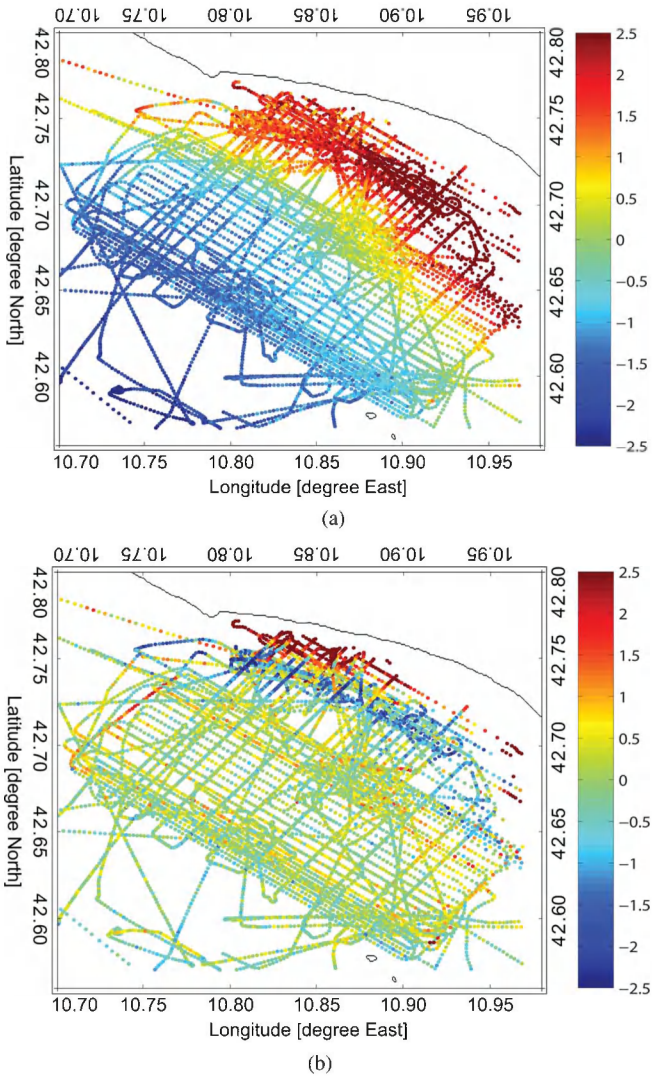

Fig. 10. Map of the two principal components that show 68% and 25% of the data variability, respectively. (a) Principal component 1 (68%). (b) Principal component 2 (25%).

The PCA has been applied to assess the three signal feature combinations that contain the relevant information for discriminating between different bottom types. Two (out of three) principal components, which show approximately 68% and 25% of the variability of the data, are used for clustering analysis. They are given in Fig. 10. The first principal component is influenced by all three features, i.e., in decreasing order energy, time spread, and skewness, whereas the second principal component is dominated by the skewness and time spread. Based on the inspection of the first two principal components, the number of clusters with similar acoustic properties was set to four. The resulting classification map is given in Fig. 11.

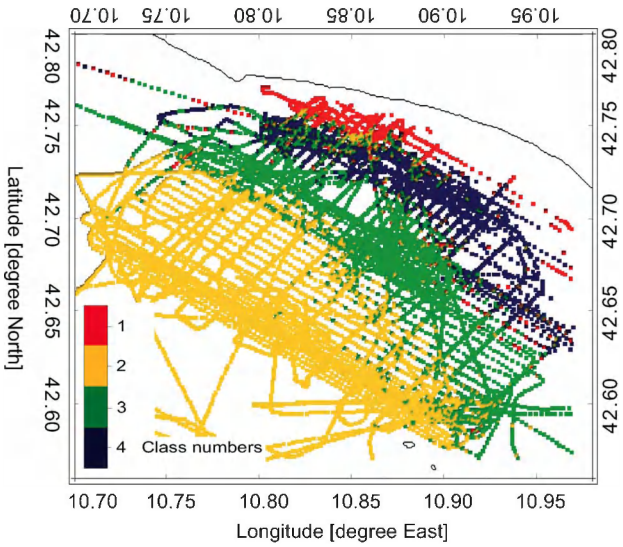

Fig. 11. Classification results of the PCA and cluster analysis using SBES signal features (energy, time spread, and skewness) at 200 kHz.

TABLE V
CORRELATION BETWEEN THE SBES SIGNAL PARAMETERS

	Energy	Time spread	Skewness
Energy	1.0000	-0.7121	-0.5511
Time spread	-0.7121	1.0000	0.2757
Skewness	-0.5511	0.2757	1.0000

Independent information about the acoustic properties of the seafloor is available through the MBES data set (Fig. 9). Both classification results match quite well. Although this is expected based on the fact that similar frequencies are used, one still has to consider that the measurement systems are quite different. The SBES is measuring only at angles close to nadir, whereas the MBES measurements used for the classification are all taken at grazing angles. From the current analysis, it can be concluded, therefore, that the different seafloor types, present in the area, affect both the measurements of nadir and the more grazing angles.

V. SEISMIC ANALYSIS

A seismic survey was carried out at the experimental site to obtain a picture of the sediment layering. A large number of tracks have been sailed and are indicated in Fig. 1. Two different systems have been employed, i.e., the X-STAR and the UNIBOOM. In the following, a detailed description of four selected seismic profiles is given. The corresponding transects have been selected such that they surround the experimental area. Figs. 12 and 13 present the measurements.

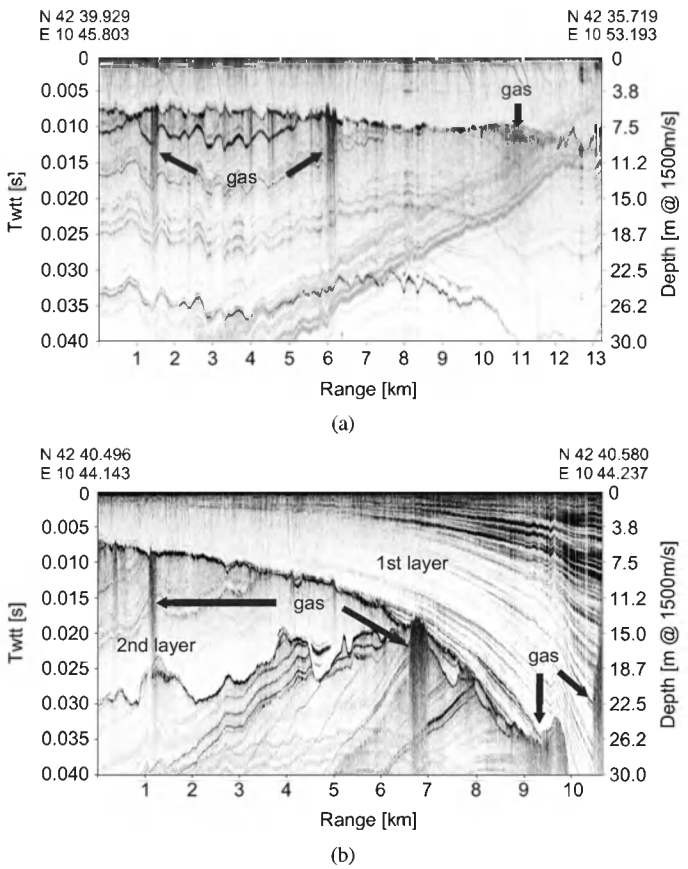

Fig. 12. Comparison of two seismic X-star profiles: profile AB lies in the deep part of the MREA/BP'07 area and runs parallel to the coastline; profile CD runs perpendicular to it. Both profiles start at zero two-way travel time (Twtt) at the water–sediment interface. (a) X-Star profile AB. (b) X-Star profile CD.

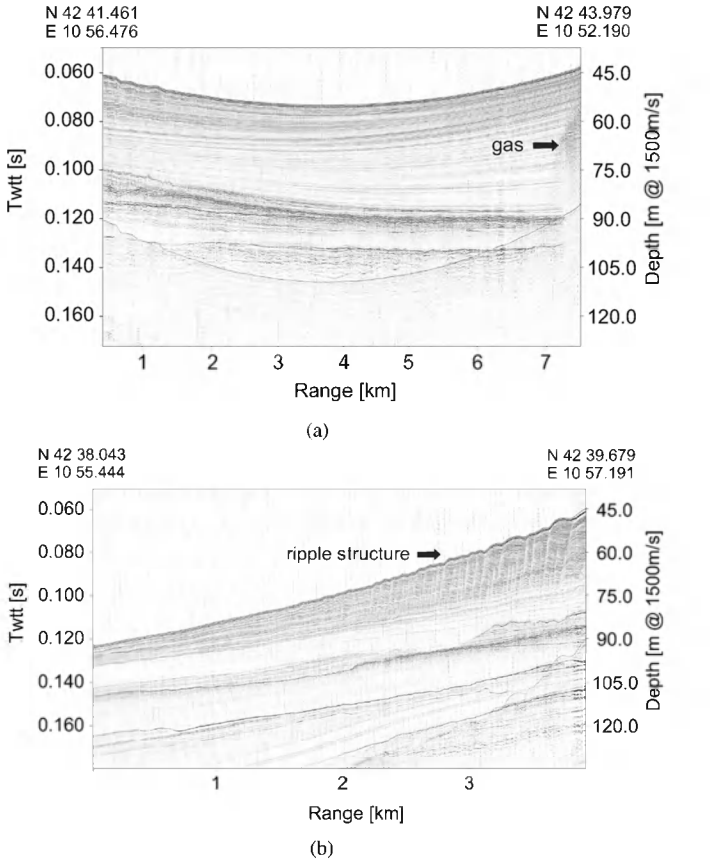

Fig. 13. Comparison of two Uniboom profiles: profile 13 lies in the shallow part of the MREA/BP'07 area and runs parallel to the coastline; profile 11 runs perpendicular to it. Both profiles have zero two-way travel time (Twtt) at source depth. (a) Uniboom profile 13. (b) Uniboom profile 11 (shallow part).

The two profiles presented in Fig. 12 were recorded by the X-STAR. Their position and orientation (respectively, parallel and perpendicular to the coastline) are displayed in Fig. 14. The two UNIBOOM profiles, which are shown in Fig. 13, are those of legs 13 and 11. Their position and orientation again are displayed in Fig. 14.

The seismic profiles indicate that a sediment layer of variable thickness is present in all profiles. The thickness of the layer varies with distance to the coast. In the shallow-water area, this thickness amounts to 40 m and more, whereas it amounts to only about 5 m in the deepest part. From the analysis of the sediment samples, this layer is known to consist of very fine material. Underneath this upper sediment layer additional layering is present. Another feature indicated by the seismic measurements is the presence of gas. Gas is found in the shallowest parts of the research area as well as at a few other spots in the deeper parts. The positions where gas is visible are indicated in Figs. 12 and 13. The gas mainly remains below the first sediment layer. However, this does not hold for the shallow coastal area, where gas reaches the water–sediment interface. Here also the largest amount of gas is detected.

As a next step, all seismic measurements have been combined. Based on all these results, sediment thicknesses over the entire experimental are have been determined by interpolation. Fig. 14 presents these results, with layer thickness depicted in color. It is clearly seen that the behavior of the sediment thickness, as visible in the four transects of Figs. 12 and 13, is continued over the entire area. Also indicated in Fig. 14 are the positions at which gas deposits occur as the white stripes on top of the black transects. The distribution of gas deposits, as observed in the selected profiles (Figs. 12 and 13), is confirmed by other profiles, mainly taken in the northern and western part of the MREA/BP'07 area.

VI. Assessment and Interpretation of the Results

To obtain a 3-D picture of the seafloor, various data sets have been considered in the previous sections. The analysis has shown that the MREA/BP'07 area is composed of fine sediments of variable thickness on top of a second sediment layer, whose material is known from historical core samples [16] to be composed of bioclastic muddy sand and biocalcarenite.

The analysis of the MBES data indicates the existence of four acoustic classes, roughly occurring in four distinct areas. The analysis of the SBES data also indicates the existence of four acoustic classes, based on the clustered principal components (linear combination of the three echo envelope feature: energy, time spread, and skewness). Although the acoustic classes obtained by the two approaches cannot be linked directly, the spatial distribution of the classes revealed by the two approaches is

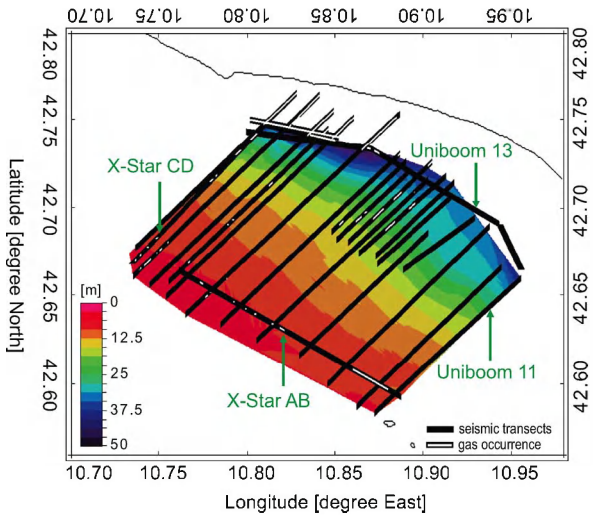

Fig. 14. Thickness (in meters) of the sediment layer in the MREA/BP'07 research area (color) and gas deposits (white lines) along the seismic transects (black lines).

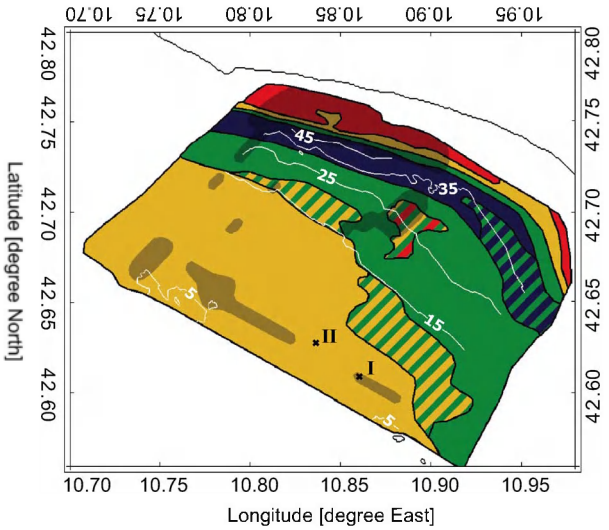

Fig. 15. Map of features obtained in the MREA/BP'07 area by merging the results from different devices (MBES, SBES, and seismic). Colors indicate the high-frequency acoustic classes. Shaded regions correspond to gas, extracted from seismic profiles. The sediment thickness, also obtained from the seismics, is given as lines of equal thickness (white lines) in steps of 10 m, starting at 5 m. Furthermore, the two sites, referred to in Section VII, are indicated by black crosses.

in very good agreement. This is further confirmed by a correlation analysis. By considering the two sets of acoustic classes at similar positions, a correlation coefficient of 0.74 is obtained.

Considering the MBES backscatter data that are used for the MBES classification, it can be concluded that the highest backscatter strengths occur close to the coast. The lowest backscatter values are found along the slope. Backscatter values are found to increase again when approaching the area with larger water depths. However, the grabs indicate a decreasing grain size, i.e., higher M_z values, when going from the coast to the deeper waters. In general, decreasing grain sizes are expected to result in lower backscatter strengths [38], contrary to the results presented here. For the present results, no direct link between mean grain size, obtained from bottom grab samples, and backscatter strength can be observed for the soft sediments present in the MREA/BP'07 area. Therefore, the increase in backscatter as observed for the deep-water area should be related to sediment parameters other than the mean grain size. An analysis of the seismic measurements revealed the presence of gas deposits in the area; see Fig. 14. Despite the sparseness of the seismic measurements, a trend can be observed with the high backscatter values being found to occur in regions where gas is present. In the southwestern part, this is accentuated by an additional increase in the backscatter strength at some of the outer beam angles, as documented in Fig. 9.

It can be concluded that the results are consistent for the different data sets. Especially the backscatter strength and slope from the MBES measurements and the cluster from the SBES analysis show the same trend. The gas deposits extracted from the seismic data mainly agree with regions of increased backscatter strength. However, due to sparse sampling, regions in which no gas is shown have to be assessed with caution, although most of the seismic profiles show the same trend in gas occurrence.

Features obtained from the different types of measurements are combined in Fig. 15 to indicate regions in which acoustic signals might be affected by other phenomena than sediment type, e.g., gas or sediment thickness. This information can be used for selecting specific locations for geoacoustic inversion runs.

The colors in Fig. 15 represent the acoustic classes according to high-frequency systems (mainly MBES), interpolated over the area under study. The two- and three-color dashed regions indicate areas in which two or three types of acoustic classes occur next to each other on a small scale. These regions are partly related to features on the seafloor. For example, the regular structure close to the Ombrone estuary is revealed in the dashed blue/green region. High slope values ($> 2^\circ$), which are not shown in this figure, mainly occur in this part and in the blue colored region. Also shown are the lines of equal sediment thickness, which are plotted in white. The shaded areas indicate gas in both the first and/or second sediment layer.

VII. Application of the Results

The consistency between the sediment characterization obtained from the MBES, SBES, and seismic measurements is such that we conclude that Fig. 15 (obtained from these measurements) can serve as basis for subseafloor sediment classification techniques; e.g., areas of interest that require further assessment can be selected from this figure.

In this section, we make a first step towards these applications. For this purpose, data from a hydrophone array at two sites are selected according to their difference in sediment type. These sites are indicated in Fig. 15 by I and II. To eliminate the effect of other parameters, measurements are considered that are taken in areas with equal water depths ($\sim$105 m) and equal source and receiver geometry.

The hydrophone arrays were allowed to drift over the area for limited periods of time. Considered measurements are the arrivals corresponding to 0.8–1.6-kHz chirp transmissions received at the deepest hydrophone (35 m).

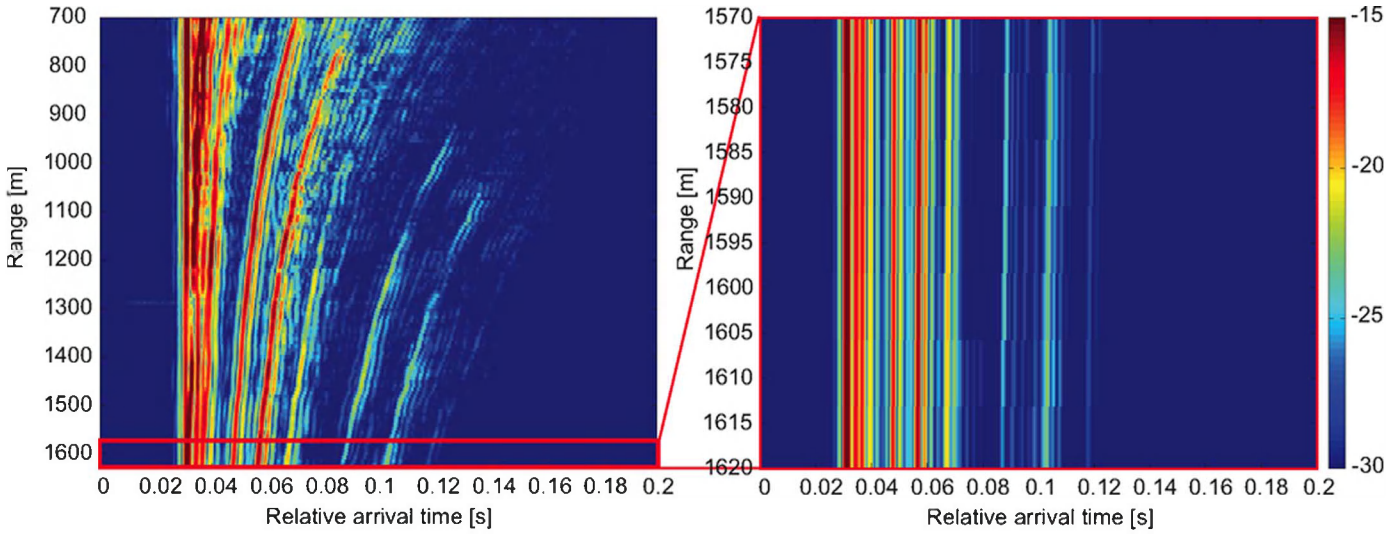

(a)

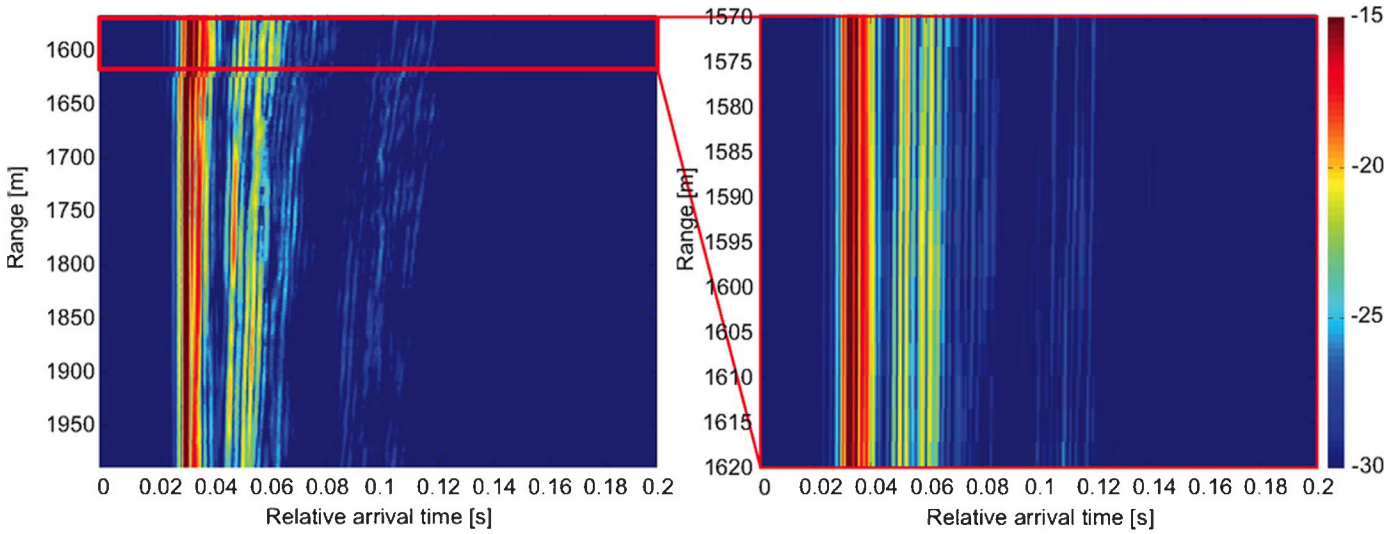

(b)

Fig. 16. Matched-filtered signal in decibel units, obtained at the deepest hydrophone (35 m) of a four-element vertical array at two different sites (site I contains diffuse gas in the seafloor; site II shows no gas in the seafloor). The left-hand side part gives matched-filtered signals during the entire run. The right-hand side part zooms into ranges of 1570–1620-m distance from the source. (a) Site I. (b) Site II.

The matched-filtered received signals are depicted in Fig. 16 for the two sites. The left-hand side plots show the received signals for the entire run, whereas the plots on the right-hand side show in detail those parts of the received signals that are available at the same ranges (1570–1620 m) and, therefore, employed for comparison. The ranges have been calculated from the first arrivals, which result from almost direct paths through the water column. The later arrivals are due to multipath effects and have undergone significant interaction with the sea bottom. Therefore, they are of interest for sediment classification purposes. Signals acquired at site I show stronger late arrivals than those acquired at site II, indicating higher contrast at the water–sediment interface for site I compared to site II.

From Fig. 15, the bottom in area I is known to contain diffuse gas. This is not the case for the bottom of area II. The gas is expected to result in increased impedance contrast between the water and the sediment, which is in agreement with the stronger later arrivals at site I. Although having undergone interaction with the sea bottom, the late arrivals could not be linked to mean grain size, since no difference between the grain sizes could be observed in the bottom grab data at the two sites. In contrast, this difference between the two sites is evident in the combined acoustic classification, presented throughout this paper. This demonstrates the strength of the chosen approach.

Inversions will be carried out to further validate the hypothesis that gas is the factor affecting the signals received at the hydrophone arrays.

VIII. Conclusion

In this paper, the results of an effort to characterize the sediments in a coastal environment by combining different acoustic

remote sensing techniques are presented. High-frequency systems, e.g., the MBES and the SBES, have proven to provide a consistent picture of the spatial distribution of the sediments over the entire area. However, due to the high frequencies involved, this distribution is valid only for the upper centimeters of the sediments. Seismic systems have shown to give valuable additional information of the structure of the sediment body.

It was found that sediment samples could not be used for linking the acoustic classes to bottom type or mean grain size. Based on the analysis of the seismic profiles it was concluded that the existence of different classes is, at least partially, caused by the presence of gas in the sediments.

Overall, it can be concluded that the combination of MBES, SBES, and seismic measurements allows for a fast and efficient assessment of the sediment distribution in an area.

Furthermore, the relevance of the resulting sediment distribution map as a basis for subseafloor classification techniques, i.e., geoacoustic inversion, has been investigated. Based on this map, acoustic data acquired by hydrophone arrays have been selected in two areas with different sea bottom characteristics. The two selected data sets clearly show different arrival patterns. Therefore, the present approach promises to perform well as a basis for selecting areas for subseafloor sediment classification techniques, which in turn can provide complementary information about the sea bottom.

ACKNOWLEDGMENT

The authors would like to thank all individuals and institutions involved in the 2007 Maritime Rapid Environmental Assessment/Blue Planet (MREA/BP'07) Joint Research Project. Especially, the contributions of the Royal Netherlands Navy, The Netherlands Organization for Applied Research (TNO), and NATO Undersea Research Centre in the observational program are hereby deeply acknowledged. The authors would also like to thank P. Boni and P. Nardini for the processing of the seismic data and the preparation of the environmental database, respectively.

REFERENCES

[1] J.-C. Le Gac and J.-P. Hermand, "MREA/BP07 cruise report," NATO Undersea Res. Cntr., La Spezia, Italy, Tech. Rep. NURC-CR- 2007-04-1D1, Dec. 2007.

[2] L. Hellequin, J.-M. Boucher, and X. Lurton, "Processing of high-frequency multibeam echo sounder data for seafloor characterization," *IEEE J. Ocean. Eng.*, vol. 28, no. 1, pp. 78–89, Jan. 2003.

[3] G. Canepa and E. Pouliquen, "Inversion of geo-acoustic properties from high frequency multibeam data," in *Proc. Boundary Influences in High Frequency Shallow Water Acoust.*, Bath, U.K., 2005, pp. 233–240.

[4] J. M. Preston, "Automated acoustic seabed classification of multibeam images of Stanton Banks," *Appl. Acoust.*, vol. 70, no. 10, pp. 1277–1287, 2009.

[5] D. D. Sternlicht and C. P. de Moustier, "Remote sensing of sediment characteristics by optimized echo-envelope matching," *J. Acoust. Soc. Amer.*, vol. 114, no. 5, pp. 2727–2743, 2003.

[6] D. D. Sternlicht and C. P. de Moustier, "Time-dependent seafloor acoustic backscatter (10–100 kHz)," *J. Acoust. Soc. Amer.*, vol. 114, no. 5, pp. 2709–2725, 2003.

[7] P. A. van Walree, M. A. Ainslie, and D. G. Simons, "Mean grain size mapping with single-beam echo sounders," *J. Acoust. Soc. Amer.*, vol. 120, no. 5, pp. 2555–2566, 2006.

[8] J. M. Preston, A. C. Christney, W. T. Collins, and S. Bloomer, "Automated acoustic classification of sidescan images," in *Proc. IEEE OCEANS Conf.*, 2004, pp. 2060–2065.

[9] C. Flewellen, N. Millard, and I. Rose, "TOBI, a vehicle for deep ocean survey," *IEEE J. Ocean. Eng.*, vol. 5, no. 2, pp. 85–93, Apr. 1993.

[10] J.-P. Hermand and P. Gerstoft, "Inversion of broad-band multitone acoustic data from the YELLOW SHARK summer experiments," *IEEE J. Ocean. Eng.*, vol. 21, no. 4, pp. 324–346, Oct. 1996.

[11] M. Snellen, D. G. Simons, M. Siderius, J. Sellschopp, J. , and P. L. Nielsen, "An evaluation of the accuracy of shallow water matched field inversion results," *J. Acoust. Soc. Amer.*, vol. 109, no. 2, pp. 514–527, 2001.

[12] S. E. Dosso, M. J. Wilmut, and A.-L. S. Lapinski, "An adaptive-hybrid algorithm for geoacoustic inversion," *IEEE J. Ocean. Eng.*, vol. 26, no. 3, pp. 324–336, Jul. 2001.

[13] M. Siderius, P. L. Nielsen, and P. Gerstoft, "Range-dependent seabed characterization by inversion of acoustic data from a towed receiver array," *J. Acoust. Soc. Amer.*, vol. 112, pp. 1523–1535, 2002.

[14] M. R. Fallat, S. E. Dosso, and P. L. Nielsen, "An investigation of algorithm-induced variability in geoacoustic inversion," *IEEE J. Ocean. Eng.*, vol. 29, no. 2, pp. 85–93, Apr. 1993.

[15] Y.-M. Jiang and N. R. Chapman, "Bayesian geoacoustic inversion in a dynamic shallow water environment," *J. Acoust. Soc. Amer.*, vol. 123, no. 6, pp. EL155–EL161, 2008.

[16] J.-P. Hermand, "Broad-band geoacoustic inversion in shallow water from waveguide impulse response measurements on a single hydrophone: Theory and experimental results," *IEEE J. Ocean. Eng.*, vol. 24, no. 1, pp. 41–66, Jan. 1999.

[17] J.-P. Hermand and J.-C. Le Gac, "Subseafloor geoacoustic characterization in the kilohertz regime with a broadband source and a 4-element receiver array," in *Proc. MTS/IEEE OCEANS Conf.—Oceans, Poles and Climate: Technological Challenges*, Quebec City, QC, Canada, Sep. 2008.

[18] J.-P. Hermand and J.-C. Le Gac, "Toward higher acoustic frequencies and fewer hydrophones to invert for subbottom properties with underwater robots: Experimental results," in *Proc. Pacific Rim Underwater Acout. Conf., Mid to High Frequency Ocean Acoustics: Modeling, Measurement, and Applications*, 2009, pp. 79–82.

[19] M. Berrada, M. Meyer, M. Asch, J.-P. Hermand, and K. B. Smith, "Efficient semi-automatic adjoint generation and its application for implementing acoustic particle velocity in geoacoustic inversion," in *Proc. 8th Int. Conf. Theor. Comput. Acoust.*, 2007, pp. 13–21.

[20] P. D. Mourad and D. R. Jackson, "High frequency sonar equation models for bottom backscatter forward loss," in *Proc. IEEE OCEANS Conf.*, 1989, vol. 4, pp. 1168–1175.

[21] C. de Moustier and D. Alexandrou, "Angular dependence of 12-kHz seafloor acoustic backscatter," *J. Acoust. Soc. Amer.*, vol. 90, no. 1, pp. 522–531, 1991.

[22] D. G. Simons and M. Snellen, "A comparison between modeled and measured high frequency bottom backscattering," in *Proc. Eur. Conf. Underwater Acoust.*, 2008, pp. 639–644.

[23] D. G. Simons and M. Snellen, "A Bayesian approach to seafloor classification using multi-beam echo-sounder backscatter data," *Appl. Acoust.*, vol. 70, no. 10, pp. 1258–1268, 2009.

[24] O. Carrière, J.-P. Hermand, J.-C. Le Gac, and M. Rixen, "Full- field tomography and Kalman tracking of the range-dependent sound speed field in a coastal water environment," *J. Mar. Syst.* , vol. 78, Special Issue on MREA and Coastal Processes: Challenges for Monitoring and Prediction, pp. S382–S392, 2009.

[25] O. Carrière, J.-P. Hermand, and J. V. Candy, "Inversion for time-evolving sound-speed field in a shallow ocean by ensemble Kalman filtering," *IEEE J. Ocean. Eng.*, vol. 34, no. 4, pp. 586–602, Oct. 2009.

[26] F. L. Chiocci, L. Orlando, and P. Tortora, "Small-scale seismic stratigraphy and paleogeographical evolution of the continental shelf facing the SE Elba Island (northern Tyrrhenian Sea, Italy)," *J. Sedimentary Pedrology*, vol. 61, no. 4, pp. 506–526, 1991.

[27] National Geophysical Data Center, "Topographical data," Boulder, CO, last viewed Jul. 7, 2009 [Online]. Available: http://www.ngdc.noaa.gov/mgg/global/global.html

[28] National Geophysical Data Center, "Coastline extractor," Boulder, CO, last viewed Jul. 7, 2009 [Online]. Available: http://rimmer.ngdc.noaa.gov

[29] C. K. Wentworth, "A scale of grade and class terms for clastic sediments," *J. Geology*, vol. 30, pp. 377–392, 1922.

[30] R. L. Folk and W. C. Ward, "Brazos River bar: A study in the significance of grain size parameters," *J. Sedimentary Petrology*, vol. 27, no. 1, pp. 3–26, 1957.

[31] T. F. Coleman and Y. Li, "An interior trust region approach for nonlinear minimization subject to bounds," *SIAM J. Optim.*, vol. 6, no. 2, pp. 418–445, 1996.
[32] C. L. Lawson and R. J. Hanson, *Solving Least-Squares Problems*, ser. Automatic Computation. Englewood Cliffs, NJ: Prentice-Hall, 1995, ch. 23, sec. 3.
[33] A. Amiri-Simkooei, M. Snellen, and D. G. Simons, "Using MBES for classification of riverbed sediments," in *Proc. Eur. Conf. Underwater Acoust.*, 2008, pp. 611–616.
[34] K. Siemes, M. Snellen, D. G. Simons, and J.-P. Hermand, "Using MBES backscatter strength measurements for assessing a shallow water soft sediment environment," in *Proc. IEEE OCEANS Conf.*, Bremen, 2009, DOI: 10.1109/OCEANSE.2009.5278279.
[35] P. A. van Walree, J. Tegowski, C. Laban, and D. G. Simons, "Acoustic seafloor discrimination with echo shape parameters: A comparison with the ground truth," *Continental Shelf Res.*, vol. 25, pp. 2273–2293, 2005.
[36] I. Jolliffe, *Principal Component Analysis*, 2nd ed. New York: Springer-Verlag, 2002, ch. 1–6.
[37] G. A. F. Seber, *Multivariate Observations*. New York: Wiley, 1984, ch. 7.5.
[38] Applied Physics Laboratory, University of Washington (APL-UW), "High-frequency ocean environmental acoustic models handbook," Seattle, WA, Tech. Rep. APL-UW TR 9407AEAS 9501, Oct. 1994.

Kerstin Siemes received the Dipl.-Ing. degree in geodesy from Bonn University, Bonn, Germany, in 2007.

In 2007, she joined the Acoustic Remote Sensing Group, Faculty of Aerospace Engineering, Delft University of Technology, Delft, The Netherlands, where she started her Ph.D. research in the field of underwater acoustics. This research is carried out in cooperation with the Université libre de Bruxelles (U.L.B.), Brussels, Belgium.

Mirjam Snellen received the M.Sc. degree in aerospace engineering from the Delft University of Technology, Delft, The Netherlands, in 1995 and the Ph.D. degree in geoacoustic inversion from the University of Amsterdam, Amsterdam, The Netherlands, in 2002.

She was a Research Scientist at The Netherlands Organization for Applied Research (TNO), where she was working in the group of underwater acoustics and in the group of aeroacoustics until 2003. Currently, she is the Assistant Professor in the Acoustic Remote Sensing Group, Faculty of Aerospace Engineering, Delft University of Technology, Delft, The Netherlands.

Ali R. Amiri-Simkooei graduated from the Mathematical Geodesy and Positioning Group, Faculty of Aerospace Engineering, Delft University of Technology, Delft, The Netherlands.

His research area focused on least squares variance component estimation with applications to global positioning system (GPS) data. He is an academic staff member of the Faculty of Engineering, University of Isfahan, Isfahan, Iran. Currently, he is also a Postdoctoral Researcher at the Acoustic Remote Sensing Group, Faculty of Aerospace Engineering, Delft University of Technology. His research area focuses on seafloor classification using multi- and single-beam echosounders.

Dick G. Simons received the M.Sc. degree in physics and the Ph.D. degree from the University of Leiden, Leiden, The Netherlands, in 1983 and 1988, respectively. His Ph.D. research topic involved the development of an imaging gas scintillation spectrometer for X-ray astronomy.

In 1990, he joined the Underwater Acoustics Group, Physics and Electronics Laboratory, The Netherlands Organization for Applied Scientific Research (TNO), The Hague, The Netherlands. In 2003, he was appointed part-time Professor at Delft University of Technology, Delft, The Netherlands, holding the chair "Seafloor Mapping" at the Faculty of Aerospace Engineering. In 2006, he became Full Professor, holding the chair "Acoustic Remote Sensing." He is involved in several extensive research projects characterized by a strong international cooperation and major field experiments at sea. His current research comprises the mapping of seafloor topography and composition, and its dynamic behavior, using all kinds of sonar systems, such as single- and multibeam echosounders, low-frequency active sonar, and seismic systems. He also works on geoacoustic inversion with global optimization methods such as genetic algorithms, both using active sound sources and ambient noise.

Prof. Simons is member of several committees, including the scientific committee of the European Conferences on Underwater Acoustics (ECUA). He is an Associate Editor of the IEEE JOURNAL OF OCEANIC ENGINEERING for the areas bathymetry surveys, mapping, remote sensing, and sonar image processing.

Jean-Pierre Hermand (M'86–SM'05–F'09) received the Ingénieur Civil degree in electrical and mechanical engineering and the Ph.D. degree in applied sciences from the Université libre de Bruxelles (U.L.B.), Brussels, Belgium, in 1981 and 1994, respectively.

Between 1985 and 2000, he has held several positions at the SACLANT Undersea Research Centre, La Spezia, Italy, conducting experimental and theoretical research in ocean acoustics with emphasis on inverse problems. In 1991, he became the Principal Investigator of a grant from the U.S. Office of Naval Research to develop environmentally adaptive sonar processing at the Naval Underwater Systems Center, New London, CT. In 1993, he was appointed Principal Scientist to the SACLANTCEN Environmental Research Division to lead the research and development of remote sensing techniques and inversion methodologies for the geoacoustic characterization of marine sediments. He has been Chief Scientist of many multidisciplinary experiments at sea. Currently, he is Professor and Research Director at the Université libre de Bruxelles, where he founded the Environmental Hydroacoustics Laboratory. Since 2001, he has been coordinating research activities on ocean acoustic observatories, shallow-water tomography, and data assimilation in the framework of European and international projects. His current research interests lie in adjoint modeling, Bayesian estimation, and the integrated use of acoustics to remotely sense and characterize ocean to very shallow aquatic environments, and in particular, seagrass habitats and river sediment dynamics.

Dr. Hermand is a Fellow of the Acoustical Society of America. He is currently the IEEE Vice-Chair of the Oceanic Engineering Society (OES) Technical Committee on "Sonar Signal and Image Processing."